Hindawi
Shock and Vibration
Volume 2022, Article ID 4814039, 16 pages
https://doi.org/10.1155/2022/4814039

Research Article

Analysis of Antideformation and Antivibration Effect of Different Track Beds under Subway Train Vibration

Jin Zhang,[1] **Chuanhao Xi**,[1] **Yanhua Sun**,[2] **Guangsheng Li**,[3] **Junwei Liu**,[1] **and Mengxue Wang**[1]

[1]*College of Civil Engineering, Qingdao University of Technology, Qingdao 266033, China*
[2]*School of Civil Engineering, Guizhou University of Engineering Science, Bijie 551700, Guizhou, China*
[3]*The Fourth Construction Co, Ltd of Construction Eighth Engineering Division, Qingdao 266100, China*

Correspondence should be addressed to Yanhua Sun; sunyanhuasyh@163.com

Received 22 December 2021; Accepted 17 January 2022; Published 4 February 2022

Academic Editor: Gan Feng

Running metro trains would inevitably influence the vibration deformation in the lower part of the roadbed structure. In order to study the effects of vibration, Qingdao metro line 3 tunnel was taken as the research background. The track coupling model was established using Abaqus-Simpack to analyze the train velocity, train axle load, and trackbed vibration forms for the vertical deformation of roadbed calendar effect to provide the reference in practical engineering design and deformation control. According to the analysis, influenced by the formation of Qingdao Metro Line 3, the time-history curve of the displacement excitation of the trackbed presents the distribution law of "large in the middle and small at both ends." According to the sensitivity analysis, the deformation of the trackbed is most obviously affected by the form of trackbed; the second was the influence of the axle load of the train. The speed change of the subway train presented relatively little influence on the displacement of the trackbed. Although the deformation control ability of the integral trackbed was better, its vibration reduction performance was poor. The vibration reduction performance of the rubber cushion floating trackbed was the best, followed by the steel spring floating trackbed.

1. Introduction

With the development of transportation, the vibration influence of rail train operation on the surrounding environment cannot be ignored. Many scholars have done a lot of research on this issue. He and Cui [1] used numerical simulation to research the difference of vibration law between train operation and frozen soil and undisturbed soil. Forrest and Hunt [2] established a three-dimensional numerical model to research the propagation rule of the influence of urban subway operation on tunnel structure and soil layer vibration. Yaseri et al. [3], Gao et al. [4], Zhu et al. [5], and Nejati et al. [6] researched the law of the influence of train operation on ground vibration using numerical simulation. Wang et al. [7] proposed a calculation method to analyze the full-scale three-dimensional random vibration caused by railway traffic, which could effectively solve the train-track-soil coupled vibration problem. Zhu et al. [8] proposed a method to establish a numerical model of sandstone using a two-dimensional particle flow code and a new contact model, providing a reference for the numerical simulation analysis of sandstone tunnel vibration. Yan et al. [9], Connolly et al. [10] Sanayei et al. [11], and Lopes et al. [12] researched the propagation characteristics of vibration influence on existing buildings under train operation. Based on wheel-rail interaction, Cai et al. [13] carried out dynamic simulation calculations for trains, tracks, and bridges through the TTBSIM simulation program. Dapeng et al. [14] established a three-dimensional finite element model to analyze the influence characteristics of train operation on existing foundation pits. Ma et al. [15] used finite element software to simulate and study the vibration characteristics of high-speed train operation on buildings along the line in the soft soil area of Tianjin Binhai New Area. Qiu et al. [16]

studied the vertical vibration displacement, dynamic stress, vibration acceleration, and transverse stress distribution of the upper surface layer of the train foundation bed at different speeds using layered system theory and the finite element method. Kaynia et al. [17] studied the influence of different train speeds on the ground vibration response using the finite-infinite element method. Liu et al. [18] and Han et al. [19, 20] established a three-dimensional finite element model and used dynamic implicit analysis to analyze the variation rule of ground vibration intensity under different shield tunnel burial depths, different elastic modulus of tunnel foundation, different subway train speeds, and different soil properties of tunnels. Xie et al. [21] and Liang et al. [22] established a two-dimensional finite element dynamic analysis model and studied the vibration response law of subway operation on adjacent sensitive buildings and the influence of foundation form on vibration by taking speed as the control physical quantity. Actual measurement and experimental research have been done by scholars [19, 23–26]. Schillemans et al. calculated the trainload through the measured transfer function and established a two-dimensional finite element model to study the impact of environmental vibration caused by high-speed railway train operation and analyze the vibration reduction effect of vibration reduction type floating slab track. The following was known from existing research: at present, the research mainly focused on the vibration law of the train operation on the ground, soil layer, and existing building structures. The influence of train operation on the vibration of the trackbed, which was the supporting structure of the track train, cannot be ignored. Based on the existing research, this article comprehensively considered the numerical calculation accuracy and calculation speed. Abaqus-Simpack was used to establish the rigid and flexible coupling numerical model of rail to analyze the law of track vibration deformation under the conditions of train running speed, train axle load, and different modes of trackbed vibration reduction.

2. Model Building

2.1. Technical Process of Model Building. The Abaqus-Simpack joint simulation was adopted for modeling to guarantee the accuracy and velocity of calculation. The model of the superstructure was built with the multibody dynamics software Simpack, and the model of the substructure composed of rail and trackbed was built with Abaqus. The rail and trackbed generated the flexible volume substructure through finite element calculation [27]; the Abaqus-Simpack joint simulation interface was used to import the Simpack file; the coupling relationships between the two flexible structures and the existing vehicle structures were established. The modeling technical flow is shown in Figure 1.

2.1.1. Superstructure. The vehicle model was simplified as a system composed of body, hinge, constraint, and force using Simpack [28–31], where parameters of each component of the vehicle model, as shown in Tables 1–4. Qingdao Metro Line 3 adopts the marshaling method of four bullet trains and two trailers [+TC-M-M + M-M-TC+]. As shown in Figure 2, Simpack comes with five forces that both act as coupling connectors and simplify modeling and computation. Therefore, the 5 force element is used instead of the coupler.

2.1.2. Substructure. The substructure was the key to the model. To meet the stress and strain of rail and trackbed requirements, Abaqus was adopted to establish the finite element model of the substructure and conduct modal analysis for generating a flexible body [32].

To simplify the model, a 30 m long Timoshenko beam was built in Abaqus without considering the orbital joints between each segment. One hundred one master nodes were established with one master node every 0.3 m. Besides, regardless of the gap between each trackbed, a plate unit with a width of 2.7 m and a length of 30 m was established, and a total of 102 main nodes was retained. The first 30 modes of rail and trackbed, as the principal modes, were taken for the sake of conservation. The boundary only restricted the two ends of the track with six degrees of freedom. The rail and trackbed's physical parameters are shown in Table 5.

2.1.3. The Upper and Lower Structures Are Coupled. The track and trackbed in the substructure were imported into the Simpack with the Abaqus-Simpack joint simulation interface, and the track coupler was simplified as a set of springs with three-direction stiffness, damping to coupling the track and trackbed. The bottom of the trackbed was the base cushion, which was simplified as a group of springs with three-direction stiffness, damping to be connected with the base rock of the rigid body. The spring parameters of rail fasteners and different track bed bases are as shown in Table 6. The dynamic model was adopted to describe the dynamic wheel-rail interaction relationship. Hertz's nonlinear contact theory generated the coupling relationship between the wheelset and the track (the distribution law of local stress and strain produced by contact between two objects under compression). Thus, the upper and lower structures were coupled as a whole to form the vehicle-rail coupling model. The connection between every two trains and the coupling mode with the substructure is shown in Figure 3, and the model is shown in Figure 4.

2.1.4. The Orbital Irregularities Are Stimulated. The train's vibration is influenced by many factors, such as the wear between the wheel and the track, the distance error of the track, and the deviation degree of the curvature of the track. Therefore, the irregularity of the track, including vertical irregularity, horizontal irregularity, direction irregularity, and track spacing irregularity, is an essential factor affecting the accuracy of the calculation results [33–35].

To facilitate the modeling, this simulation uses the irregularity excitation spectrum by US Federal Railway Administration (FRA) in the 1980s to simulate the random vibration in train operation based on a large number of

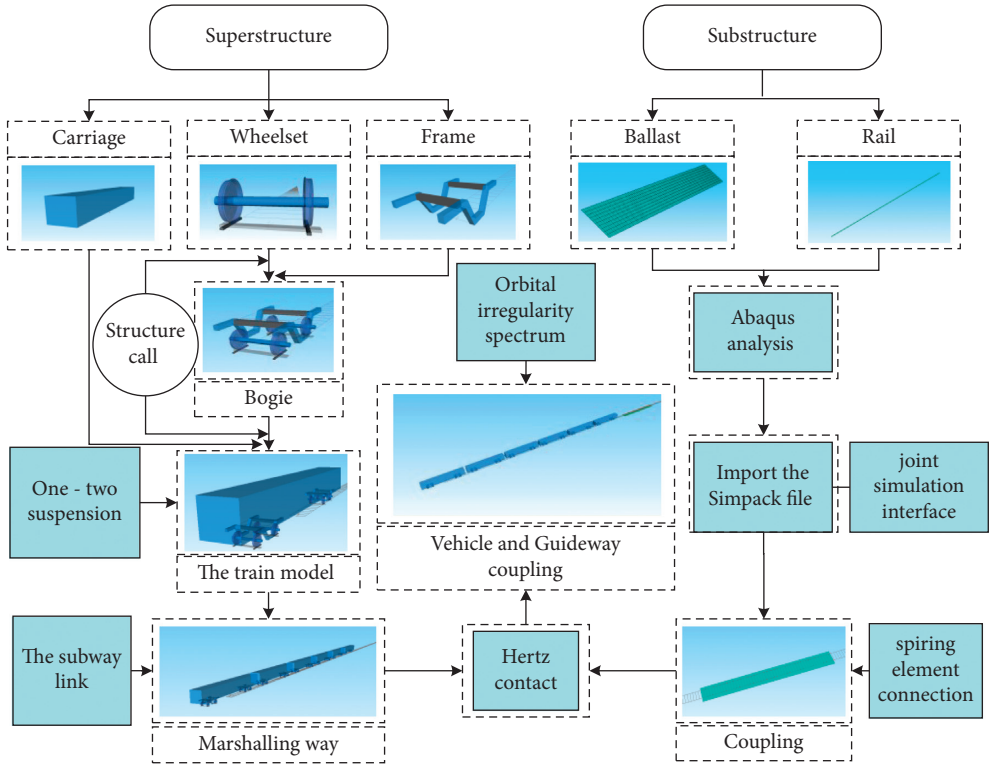

Figure 1: Technical flow route.

Table 1: Subway train body parameters.

Component	Value
Mass of subway train (t) (single cycle)	The locomotive: 36 t The trailer: 34.6 t
Subway train body length (m) (velocity direction)	19.5
Width of subway train body (m)	2.8
Height of subway train body (m) (bottom plate from top of rail: 1.1 m)	2.7 (the height of the underground train from the rail surface: 3.8 m)
Vehicle bogie distance (m), 2Lc	12.6
Bogie wheelbase fixed distance (m), 2Lt	2.2
Moment of inertia of nodding mass of subway train (kg·m^2), Iyy	1328000
Moment of inertia of mass side roll of subway train (kg·m^2), Ixx	32400
Moment of inertia of shaking head of a mass of subway train (kg·m^2), Izz	1317000

Table 2: Bogie frame parameters.

Component	Value
Quality of frame (t)A single	The locomotive: 3.6 t The trailer: 1.2 t
Length of the frame (m) (velocity direction)	2.2
Width of the frame (m)	2.05
Moment of inertia of the nodding frame mass (kg·m^2), Iyy	1760
Roll moment of inertia of frame mass (kg·m^2), Ixx	1430
Moment of inertia of shaking head of frame mass (kg·m^2), Izz	2950

measured data. The wavelength range of the spectrum was 1.524–304.8 m, and the grade of the track was divided into six levels. The maximum velocity of Qingdao Metro Line 3 is 80 km/h, which can be satisfied by the American level-5 track irrationality excitation. Therefore, the American level-5 smoothness spectrum was applied as the random external excitation of the track. The irregularity excitation spectrum relevant parameter is shown in Table 7.

Table 3: Parameters of the wheelset.

Component	Value
Quality of the wheelset (t)	1.7
The radius of the wheelset (m)	0.42
Moment of inertia of the nodding mass of the wheelset (kg·m^2), Iyy	104
Moment of inertia of the side roll of the wheelset mass (kg·m^2), Ixx	801
Moment of inertia of the wheelset mass (kg·m^2), Izz	814

Table 4: Series I and II suspension parameters.

Component	Value
Series I longitudinal stiffness (N/m)	0.96×10^6
Series I lateral stiffness (N/m)	0.96×10^6
Series I vertical stiffness (N/m)	1.2×10^6
Series I longitudinal damping (N·s/m)	2.5×10^4
Series I lateral damping (N·s/m)	2.5×10^4
Series I vertical damping (N·s/m)	5×10^4
Series II longitudinal stiffness (N/m)	0.21×10^6
Series II lateral stiffness (N/m)	0.21×10^6
Series II vertical stiffness (N/m)	0.58×10^6
Series II longitudinal damping (N·s/m)	3.5×10^4
Series II lateral damping (N·s/m)	3.5×10^4

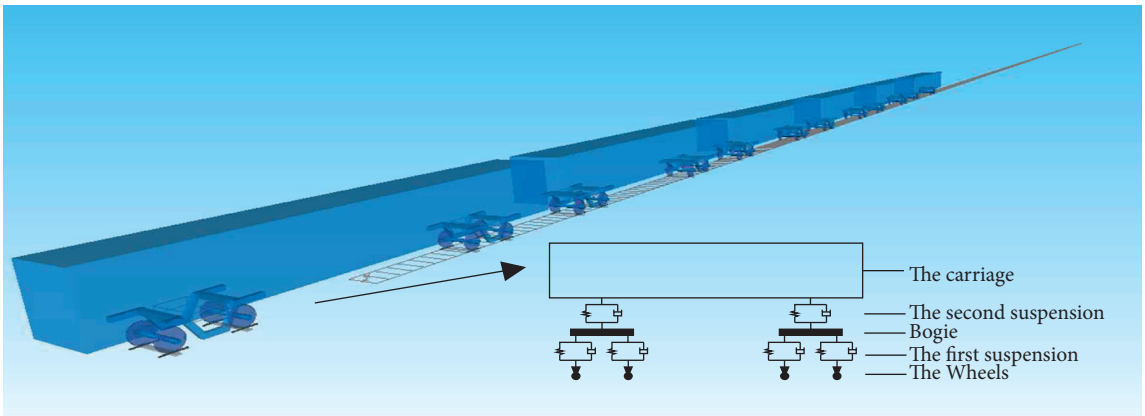

Figure 2: Subway train marshaling.

Table 5: Orbital physical parameters.

Rail	Value
Bulk density (N/m^3)	7.83×10^{11}
Mass per unit length (kg/m) (monorail)	60.64
Modulus of elasticity (Pa)	2.10×10^{11}
Poisson's ratio (μ)	0.3
Track bed	Value
Bulk density (N/m^3) (cross-sectional area1.08 m^2)	2300
Mass per unit length (kg/m) (velocity direction)	2484
Modulus of elasticity (Pa)	3.25×10^{10}
Poisson's ratio (μ)	0.25

3. Results and Discussion

3.1. Monitoring Point Selection and Simulation Scheme. Since the main displacement deformation of the substructure during train operation was vertical deformation, the rail-wheel coupling simulation calculation was mainly used to study the time-history curve of vertical displacement excitation of the trackbed and the variation rule of the trackbed. The load of the train was transmitted to the substructure through two tracks, so each vertical section had

Table 6: Parameters of the spring of the substructure.

The name of the spring	Value
Vertical dynamic stiffness of rail fasteners (kN/m)	4.2 × 103
Lateral dynamic stiffness of rail fasteners (kN/m)	9.5 × 103
Longitudinal dynamic stiffness of rail fasteners (kN/m)	4.2 × 103
Vertical damping of rail coupler (kN/m)	50
Rail coupler transverse damping (kN·s/m)	50
Longitudinal damping of rail fasteners (kN·s/m)	50
Base stiffness of integral track bed (kN/m/m2)	6.4 × 105
Base damping of integral track bed (kN·s/m/m2)	3.7
The base stiffness of rubber cushion floating plate trackbed (kN/m/m2)	2 × 104
Rubber cushion floating plate track bed base damping (kN·s/m/m2)	1 × 103
Base stiffness of steel spring floating plate trackbed (kN/m)	6.9 × 103
Steel spring floating plate track bed base damping (kN·s/m)	75

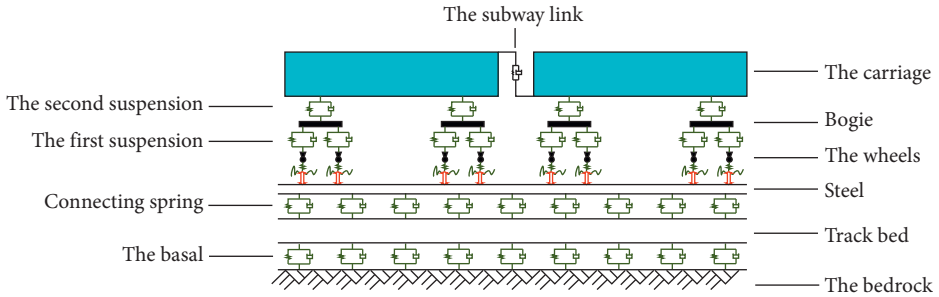

Figure 3: Vehicle-rail coupling diagram.

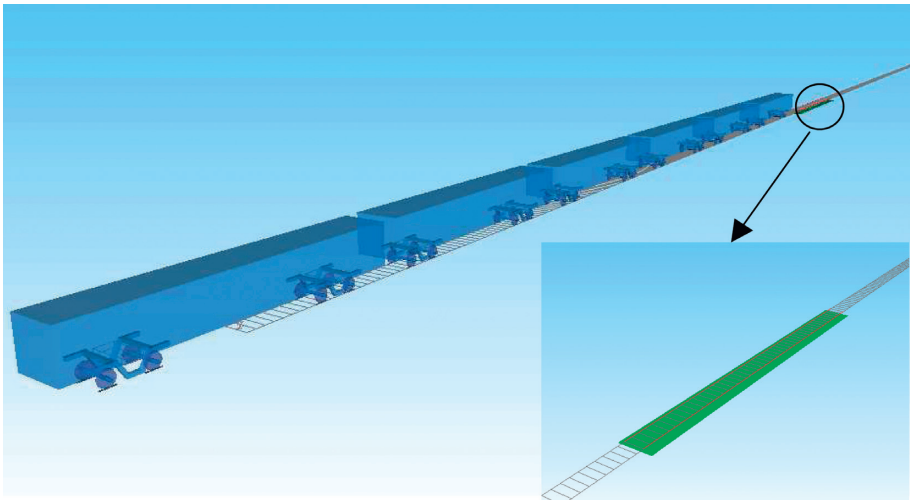

Figure 4: Effect diagram of rail coupling.

two contact points at the left side and the right side. The numerical simulation results are shown in Figures 5–10, and it is found that compared with other main nodes, the 20th pair of main nodes near the middle of the trackbed has the largest vertical displacement and time-history deformation. Therefore, the 20th pair of main nodes was taken as the object of study in simulation is shown in Figure 11, and the specific simulation scheme is shown in Table 8.

Table 7: Irregularity excitation spectrum relevant parameter.

Parameter		Parameter values of each orbital					
Symbol	Unit	6	5	4	3	2	1
A_v	$cm^2/ra\ d/m$	0.0339	0.2095	0.5376	0.6816	1.0181	1.2107
A_a	$cm^2/ra\ d/m$	0.0339	0.0762	0.3027	0.4128	1.2107	303634
Ω_s	$ra\ d/m$	0.4380	0.8209	1.1312	0.8520	0.9308	0.6046
Ω_c	$ra\ d/m$	0.8245	0.8245	0.8245	0.8245	0.8245	0.8245
Maximum running speed (km/h)		176	144	128	96	48	24

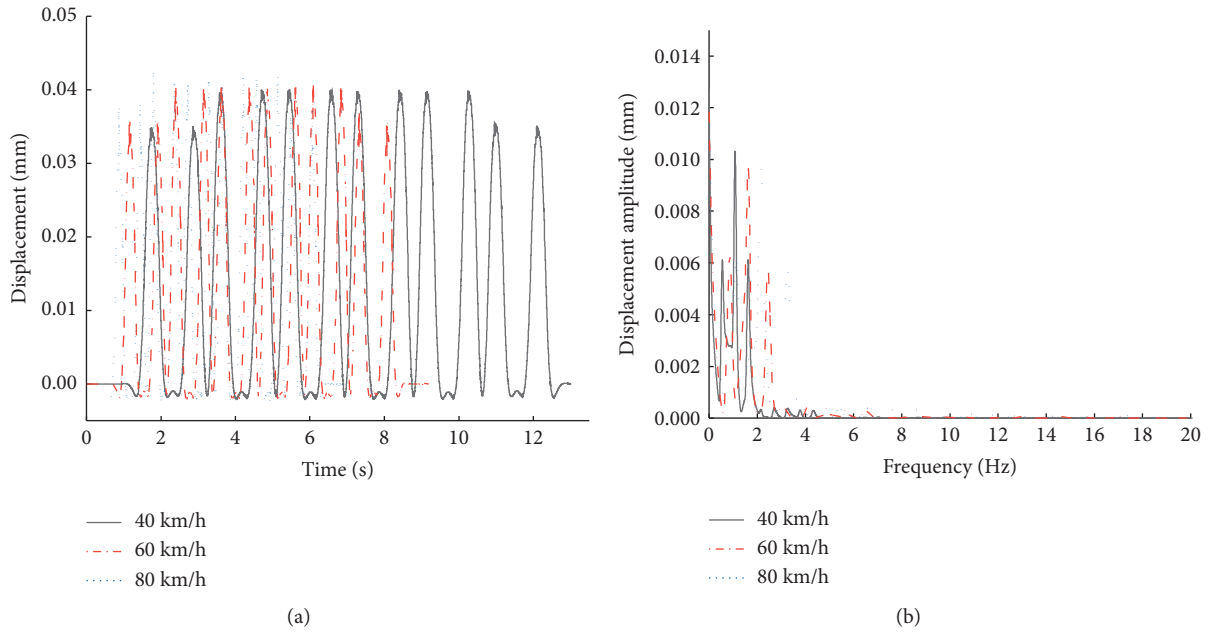

Figure 5: Vertical displacement (a) time-history curve and (b) amplitude-frequency cure of left monitoring point of trackbed at different velocities.

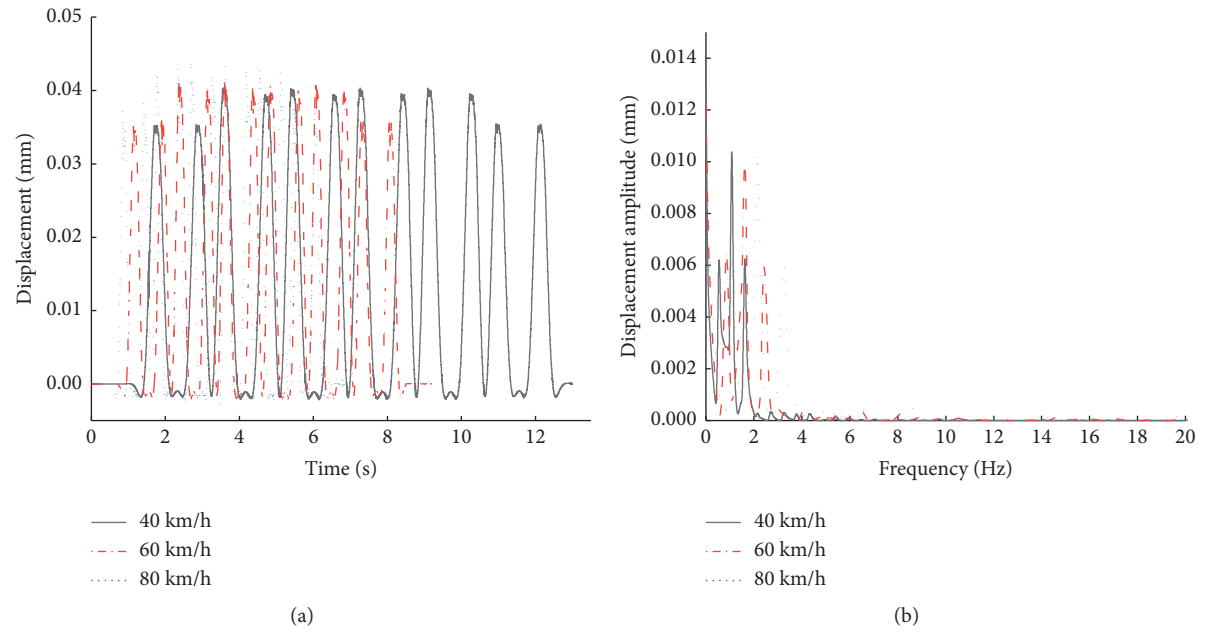

Figure 6: Vertical displacement (a) time-history curve and (b) amplitude-frequency curve of right monitoring point of trackbed at different velocities.

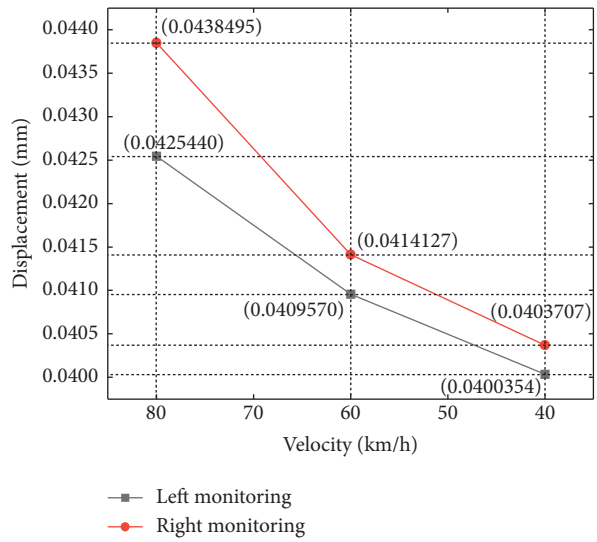

Figure 7: Comparison of maximum vertical displacement of track under different train velocities.

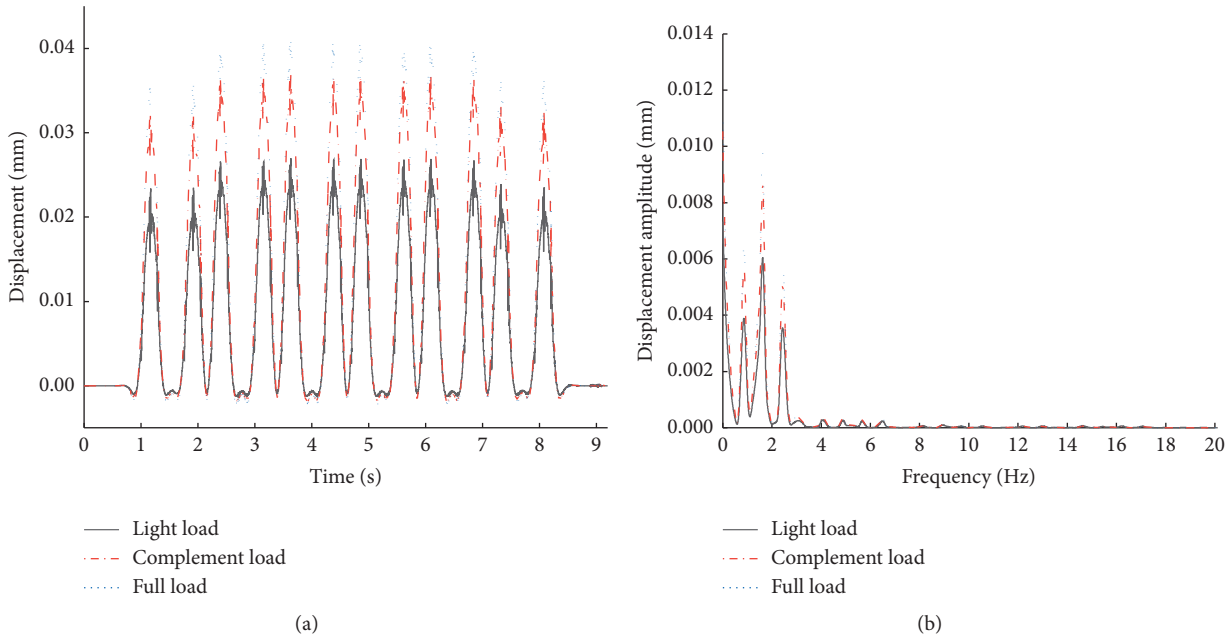

Figure 8: (a) Time-history and (b) amplitude-frequency curves of vertical displacement of left monitoring point of track bed under different axle loads.

4. Results Analysis

Most sections of Qingdao metro are integral track beds, which are adopted in this simulation when studying the influence of velocity and axle load on vertical displacement excitation.

4.1. Influence of Velocity on Vertical Displacement Excitation Time History. The simulation scheme for the influence of the train velocity on the vertical displacement excitation time history of the trackbed was conducted with the velocities of 40 km/h, 60 km/h, and 80 km/h, respectively, under the full axle load. The solve results are shown in Figures 5 and 6.

As shown in Figures 5(a) and 6(a), the vertical displacement generated by the two trailers at both ends is smaller than that generated by the four-bullet train in the middle. With the increase of velocity, the loading time of the train decreased gradually. As shown in Figure 7, under the condition of the same axle load, the maximum vertical displacement of the tunnel plate shows a nonlinear increasing trend with the increase of velocity. When the train velocity decreases from 80 km/h to 60 km/h and then from 60 km/h to 40 km/h, the vertical displacement attenuation

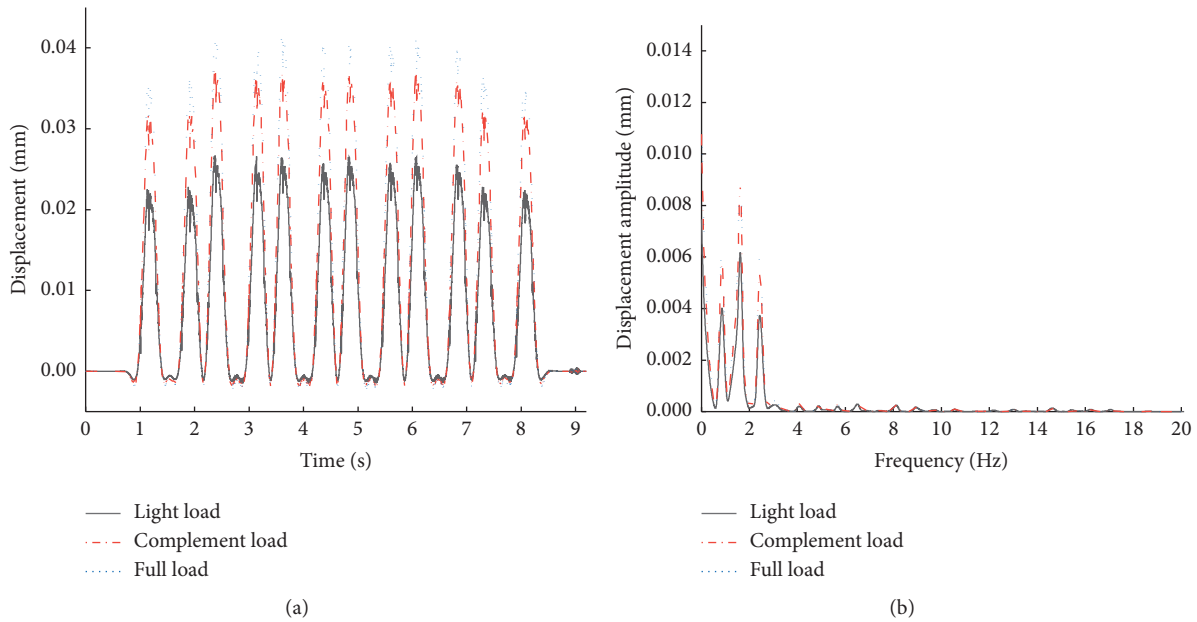

Figure 9: (a) Time-history and (b) amplitude-frequency curves of vertical displacement at the right monitoring point of trackbed under different axle loads.

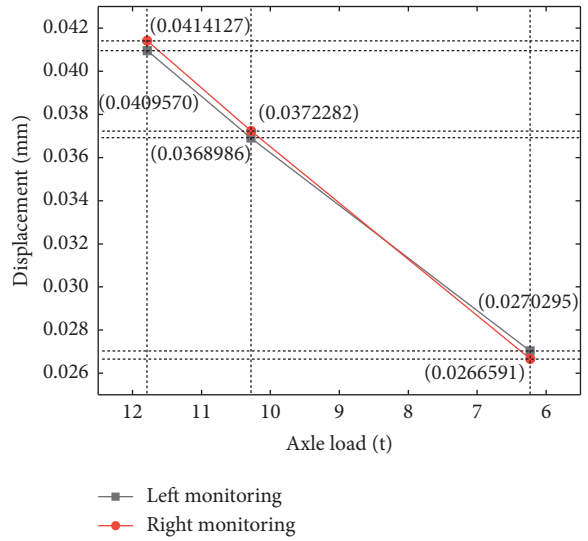

Figure 10: Comparison of maximum vertical displacement of trackbed under different axle loads.

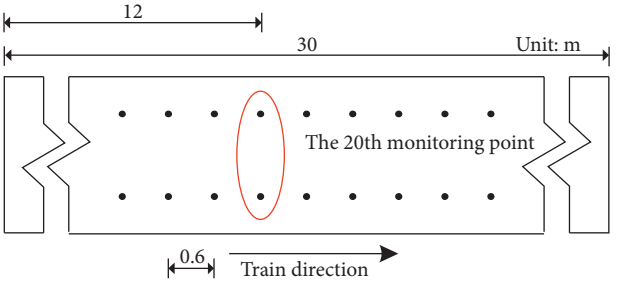

Figure 11: Position diagram of monitoring points.

Table 8: Simulation scheme.

Types of variables	Variable value
Velocity (km/h) (full load)	40 60 80
Axle load (t) (60 km/h)	6.23 (no-load) 10.28 (complement) 11.79 (full load)
Form of the trackbed	Integral trackbed Rubber cushion floating plate trackbed Steel spring floating plate bed

rate of the left monitoring point is 3.7% and 2.3%, respectively, and the vertical displacement attenuation rate of the correct monitoring point is 5.6% and 2.5%, respectively. Under the influence of velocity, the maximum values of vertical displacement excitation on the left and right sides are different, and the greater the velocity, the more pronounced the difference. As the train is affected by the irregular excitation when it is running, the train vibration shows randomness, leading to the asymmetric displacement excitation distribution on the left and right sides of the lower trackbed, which further verifies the reliability of the model. However, the attenuation rate of the left monitoring point from the velocity of 80 km/h to 40 km/h is only 5.9%, and the attenuation rate of the correct monitoring point from the velocity of 80 km/h to 40 km/h is only 7.9%. The results show that the maximum value of vertical displacement excitation is not evenly distributed due to the change of velocity, whose influence, however, is not significant.

Figures 5(b) and 6(b) show amplitude-frequency curves at different speeds. From the diagram, when the train velocity was 40 km/h, 60 km/h, and 80 km/h, the vertical displacement of the trackbed is mainly concentrated within the vibration frequency range of 0 Hz–2 Hz, 0 Hz–3 Hz, and 0 Hz–4 Hz, respectively, and each of the main frequency segments of vertical displacement amplitudes presents four peaks, all belonging to the low-frequency band. It can be found that the velocity presents an obvious influence on the vertical displacement vibration frequency range of the monitoring points on both sides. With the increase of velocity, the vertical displacement vibration frequency range expands gradually.

4.2. Influence of Axle Load on Vertical Displacement Time-History Excitation. The axle load of the train varies in different periods under the influence of the loading condition. In the morning and evening rush hours, the train is full, and the corresponding axle load is 11.79 t. At noon, there are relatively few passengers, which can be defined as the scheduled status, and the corresponding axle load is 10.28 t. When the train is about to arrive at the last station, and the passengers have almost got off the train, the axle load of the train is all provided by the components of the train itself, namely, the no-load axle load of 6.23 t. Therefore, the simulation scheme was to solve the vertical displacement excitation time-history of the trackbed caused by train vibration under full-load and no-load axle load with the velocity at 60 km/h. The solution results are shown in Figures 8 and 9.

As shown in Figures 8(a) and 9(a), the vertical displacement generated by the trailers at both ends is slightly smaller than that generated by the middle four bullet trains as a whole. With the increase of axle load, the maximum vertical displacement load shows a monotonically increasing trend. As shown in Figure 5, the maximum attenuation rates of vertical displacement of the left monitoring point of the trackbed from full load to complement load and from complement load to light load are 9.9% and 26.7%, respectively, and the maximum attenuation rates of vertical displacement of the right monitoring point of the trackbed are 10.1% and 28.4% respectively. The variation trends of the monitoring points on both sides are similar, indicating that the axial weight has little influence on the variation of the vertical displacement excitation on both sides of the trackbed at the same velocity. However, the axle load plays a crucial role in the variation of vertical displacement excitation. The attenuation rate of the left side from full-load axle load to light-load axle load is up to 34% and that of the right side from full-load axle load to light-load axle load is up to 35.6%. It can be seen that the vertical displacement excitation of the trackbed is sensitive to the axle load of the train.

As shown in Figures 8(b) and 9(b), the vertical vibration frequency of vertical displacement of the monitoring points on both sides is mainly between 0 Hz and 4 Hz, belonging to the low-frequency band with the increase of axle load; the vertical displacement of the main vibration frequency range has no obvious change. Within the frequency range of 0 Hz–4 Hz, there are four peak vertical displacement amplitudes.

4.3. Vertical Displacement and Vibration Reduction Effect of Track Bed Form. The tunnel section of Qingdao Metro Line 3 is mostly of integral type, and part of the section is made of steel spring float bed and rubber cushion float bed. To study the time-history variation rule of vertical displacement

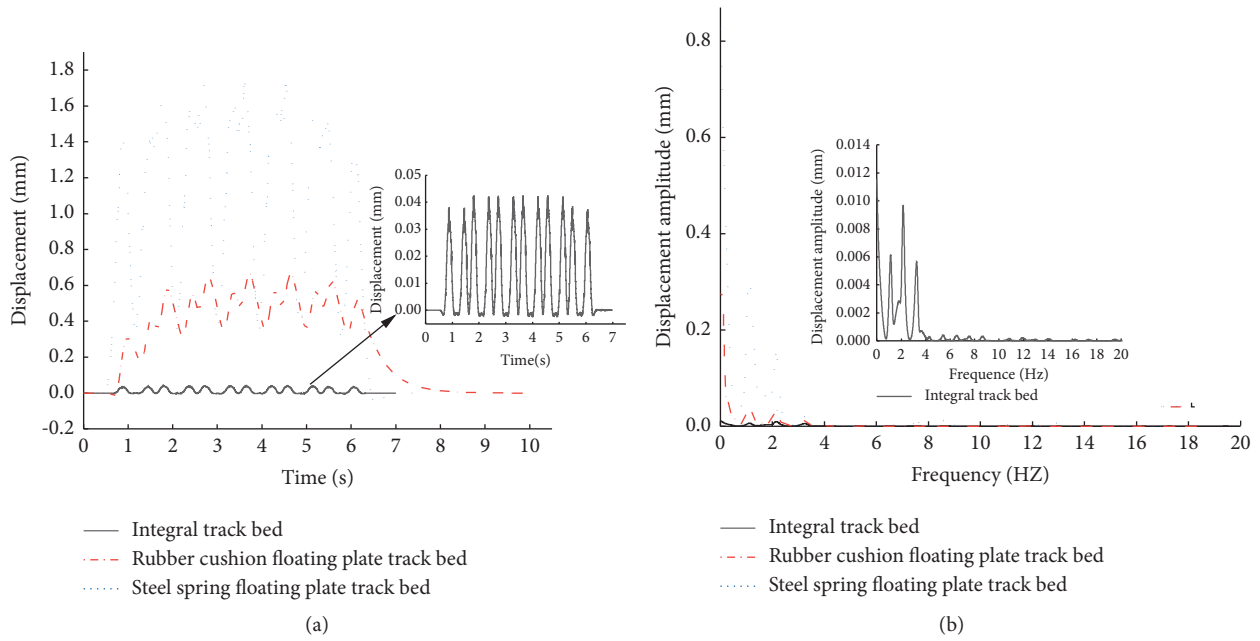

FIGURE 12: (a) Time-history and (b) frequency-history curves of vertical displacement of left monitoring point under different trackbed forms.

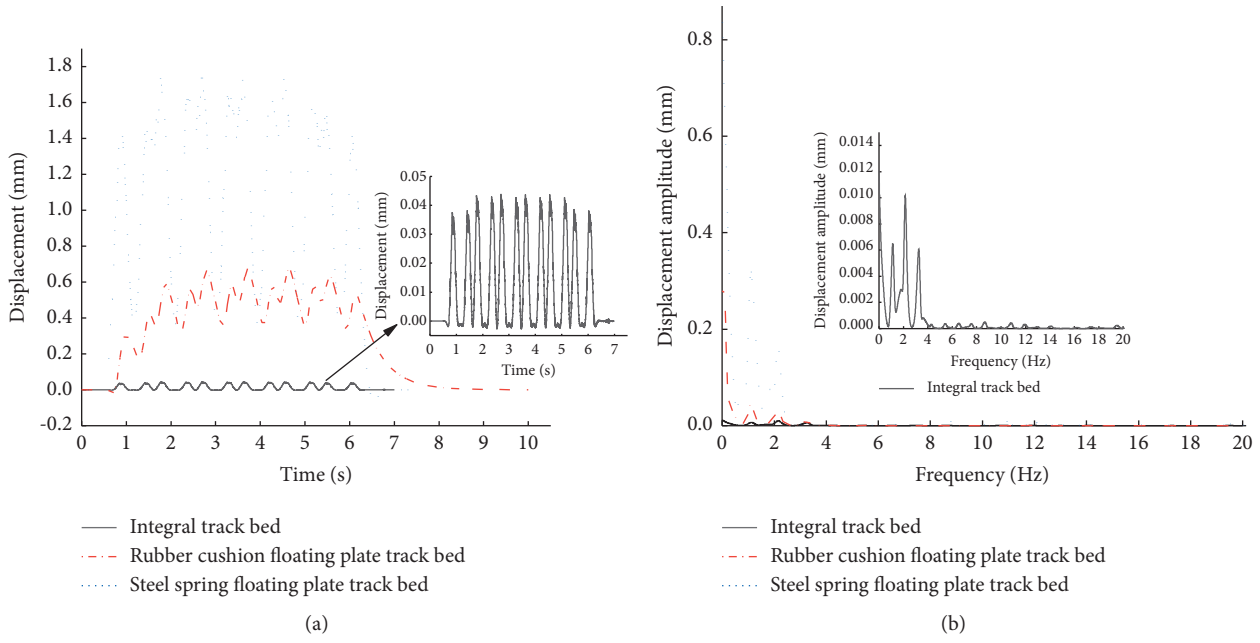

FIGURE 13: The vertical displacement (a) time-history and (b) amplitude-frequency curve of the right monitoring point under different trackbed forms.

excitation of track bed with different forms, the axial weight was set as full load and the velocity was set as 80 km/h during the simulation. The 20th pair of primary nodes of trackbed was also selected as the research object, as shown in Figure 11.

Figures 12(a) and 13(a) show the comparison diagram of the vertical displacement time history curve of different trackbed types, From the diagram, when the axle load and the velocity are the same, the time-history curve of the trackbed caused by the train vibration with different track bed forms changes significantly. As shown in Figures 13(a) and 14(a), for the trains at 80 km/h velocity, the rubber damping pad of floating plate track on displacement excitation time history is around 8.5 s. Therefore, the monolithic trackbed with steel spring floating plate track on the vertical displacement of the end of the schedule time is roughly the

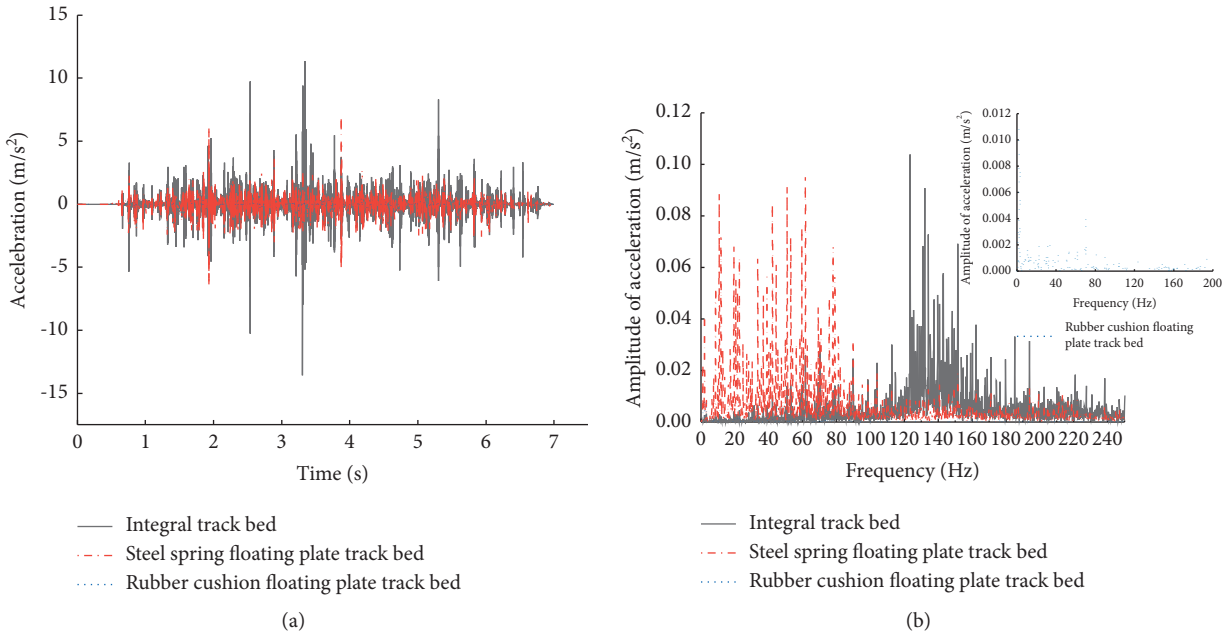

Figure 14: Acceleration (a) time-history curve and (b) amplitude-frequency curve under different trackbed forms.

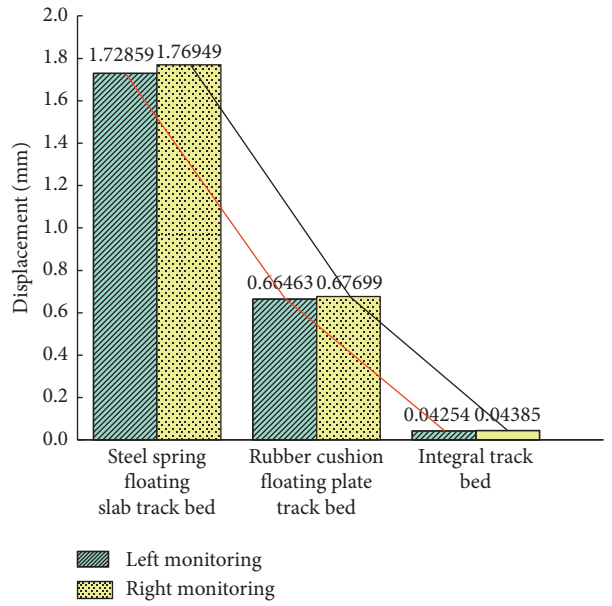

Figure 15: Maximum vertical displacement under different trackbed types.

same. For the rubber vibration isolation cushion floating plate track, though the train has been out of monitoring the position, the displacement time history of the track does not immediately end. The attenuation of vertical displacement of the trackbed is slow because the material damping of the rubber cushion floating plate trackbed is larger than that of the other two types of trackbed, and the resistance to deformation rebound is larger.

As shown in Figure 15, the change of the maximum vertical displacement produces an order of magnitude under different vibration forms. For left monitoring, steel spring floating plate trackbed on the vertical displacement of the maximum value compared to the rubber cushion floating plate trackbed on the vertical displacement of the maximum value attenuation is 61.6%; rubber cushion floating plate trackbed on the vertical displacement of the maximum value compared to the integrated track on the vertical displacement of the maximum value attenuation is 93.6%. For the right monitoring, steel spring floating plate trackbed on the vertical displacement of the maximum value compared to rubber cushion floating plate trackbed on the vertical displacement of the maximum value attenuation is 61.7%;

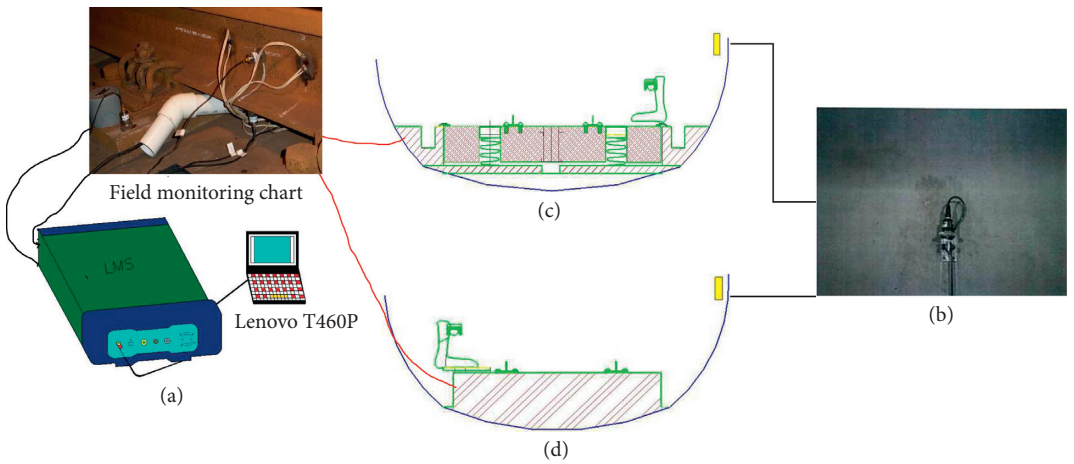

Figure 16: (a) LMS signal acquisition analyzer. (b) Vertical acceleration sensor. (c) Schematic diagram of measuring points of floating plate trackbed section. (d) Schematic diagram of measuring points of the integral trackbed section.

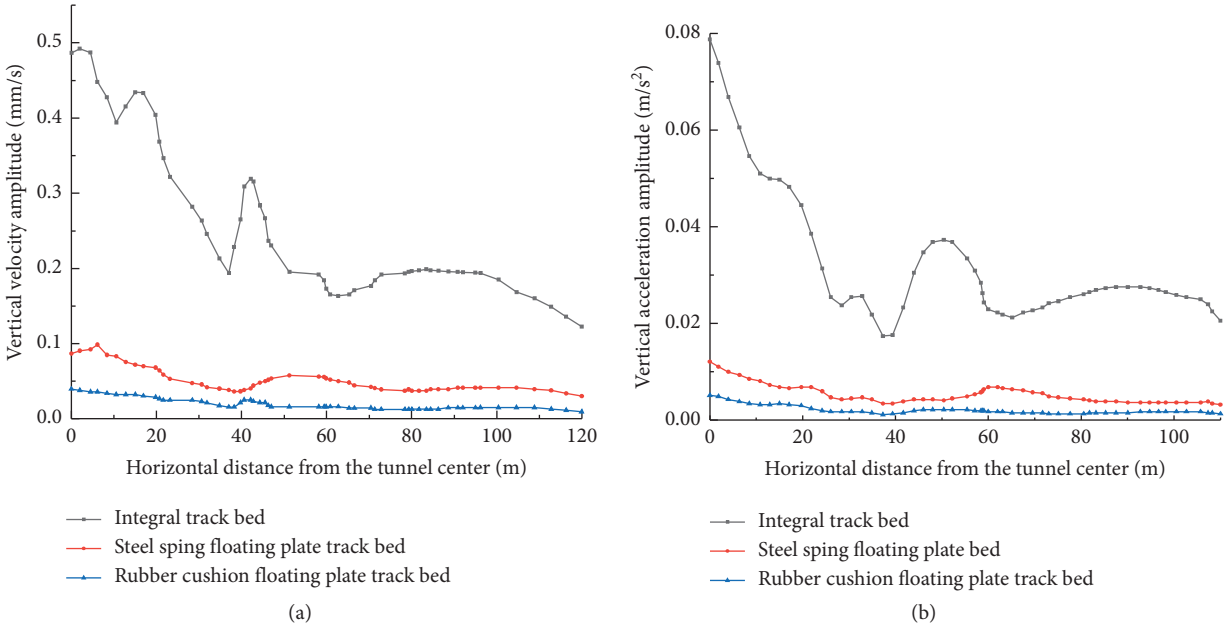

Figure 17: Vertical velocity amplitude (a) and vertical acceleration amplitude (b) varying with horizontal distance.

rubber floating plate track on the vertical displacement of the maximum value compared to integrated track on the vertical displacement of the maximum value attenuation is 93.5%. This phenomenon is because the base material of the integral trackbed was more rigid than that of the other two kinds of the trackbed and the resistance to deformation of the integral trackbed is stronger.

Figures 12(b) and 13(b) show the comparison diagram of the vertical displacement amplitude-frequency curve of different trackbed typs. From the diagram, the vertical displacement vibration frequencies of different track beds are mainly concentrated within 0 Hz–4 Hz, a low-frequency band, where the peak value of the vertical displacement amplitude of rubber damper trackbed and steel spring float trackbed appears three times, and the peak value of vertical displacement amplitude of integral track bed appear fours times.

The right monitoring points were taken as the research object when analyzing the acceleration time-history curves of different trackbed forms. As shown in Figure 14(a), the acceleration of the rubber damping cushion float bed and the steel spring float bed is attenuated compared with that of the integral track bed, indicating that the rubber cushion float bed and the steel spring float bed have a more significant effect on vibration reduction. As shown in Figure 14(b), the main frequency of acceleration of the integral trackbed is concentrated within the range of 100 Hz–200 Hz. The main frequency of acceleration of the rubber cushion floating trackbed and steel spring floating trackbed are roughly the same, both concentrating within the range of 0 Hz–100 Hz.

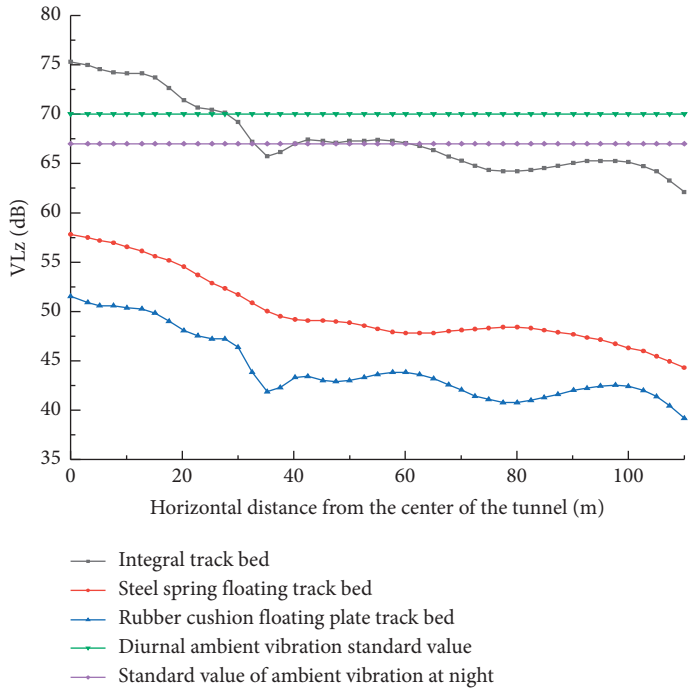

Figure 18: The variation of Z vibration level with horizontal distance.

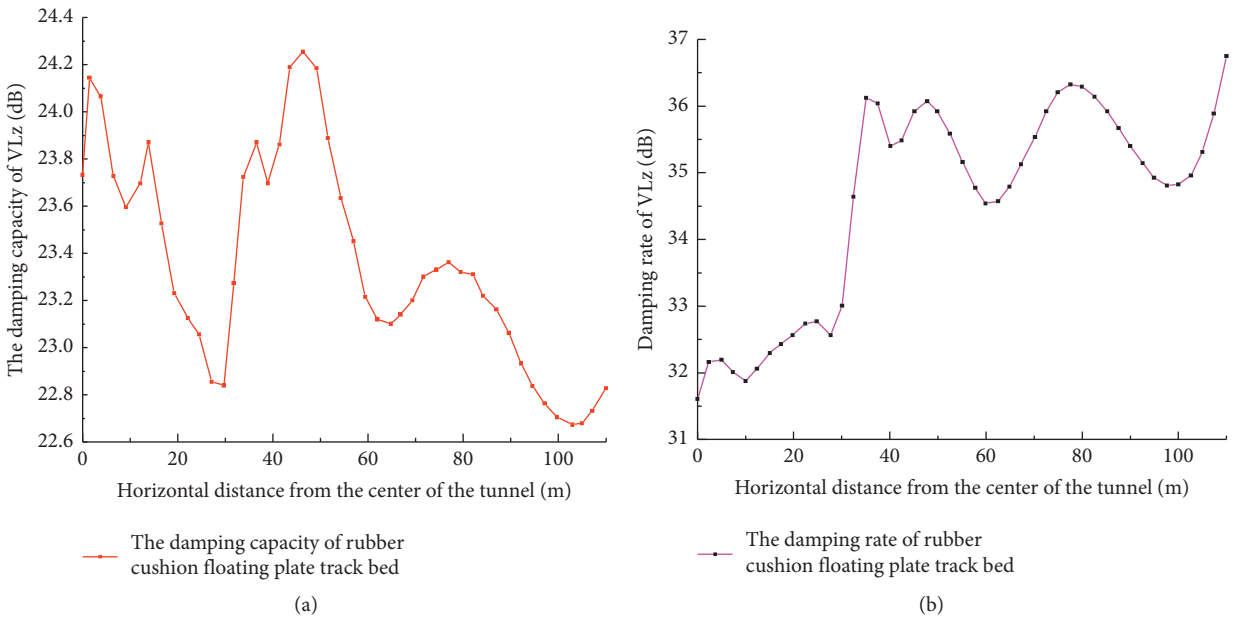

Figure 19: The variation law of damping capacity (a) and damping rate (b) of rubber cushion floating plate trackbed with horizontal distance.

5. Field Measurement Data Analysis

To preliminary verify the correctness of the model, the actual data of the Qingdao metro were used to verify the model. LMS SCADAS Mobile SCM01 information acquisition system, PCB 393A03 acceleration sensor, Lenovo T460P as the terminal, and the schematic diagram of the test equipment connection are shown in Figure 16(a). According to the requirements of Technical Specification for Floating Plate Track (CJJ/T191-2012), a vertical acceleration sensor is arranged on the tunnel wall 1.25 m away from the rail surface, as shown in Figures 16(c) and (d).

The curves of vertical velocity amplitude and acceleration amplitude with horizontal distance for different roadbed forms are shown in Figures 17(a) and 17(b). The maximum vertical vibration response appears directly above

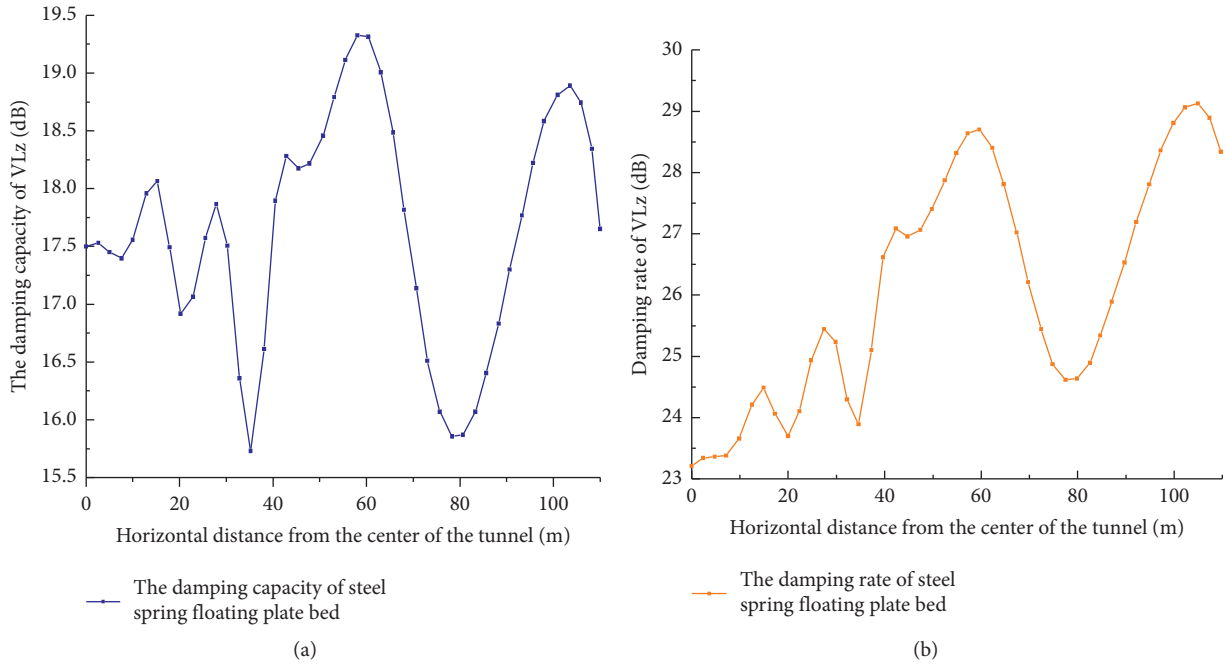

Figure 20: The variation law of damping capacity (a) and damping rate (b) of steel spring floating plate bed with horizontal distance.

the tunnel from the diagram. Moreover, there is a large area between 40 and 60 m. In other distances, the vertical vibration response generally decreases with the increase of the horizontal distance. Rubber cushion floating plate trackbed and steel spring floating plate bed structure on the vertical vibration response has pronounced attenuation effect. The two largest vertical vibration velocity amplitude attenuation rates are 92% and 83%, respectively; the largest vertical vibration acceleration amplitude attenuation rates are 93% and 84%, respectively; both numerical simulations to calculate the maximum vertical vibration velocity amplitude attenuation rate are 90% and 79%. The top amplitude attenuation rates of vertical vibration acceleration are 91% and 80%, respectively. The measured results are in good agreement with the numerical simulation results, and the damping effect of the rubber cushion floating plate trackbed on vertical vibration is slightly more significant than that of the steel spring floating plate bed.

As shown in Figure 18, with the increase of horizontal distance, the Z vibration level generally indicates a trend of gradual attenuation. Still, it is in the small amplification area between 40 and 60 m and around 90 m. The ambient vibration value caused by the integral track bed structure exceeds the standard daytime ambient vibration value by 30 m. The range of influence on the expected value of ambient vibration at night is about 60 m. The environmental vibration caused by the rubber cushion floating plate trackbed and steel spring floating plate bed structure and the integral track bed structure is below the standard value.

Figures 19(a) and 20(a) show the comparison diagram of damping capacity of rubber cushion floating plate trackbed and steel spring floating plate bed with horizontal distance. From the diagram, the maximum vibration reduction of the rubber cushion floating plate trackbed is 24.3 dB, and the ultimate vibration reduction occurs at a horizontal distance of 50 m. The minimum vibration reduction is 22.7 dB. In addition, the vibration reduction within 10 m and 40–50 m distance is significant, and the vibration reduction near 30 m is slight. The maximum vibration reduction of the steel spring floating plate bed is 19.5 dB, and the ultimate vibration reduction occurs near the horizontal distance of 60 m. The minimum vibration reduction is 15.7 dB. Additionally, the vibration reduction is more significant at the space of 50–65 m and near 100 m and smaller at the distance of 30 m and 80 m. Rubber cushion floating plate trackbed can eliminate the load generated by train operation in a short distance. As shown in Figures 19(b) and 20(b), the maximum vibration reduction rate of the rubber cushion floating plate trackbed is 37%, and the minimum vibration reduction rate is 31.5%. The maximum vibration reduction rate of the steel spring floating plate bed is 29%, and the minimum vibration reduction rate is 23%. The damping capacity and damping rate of the rubber cushion floating plate trackbed at the tunnel center are 23.76 dB and 31.56%, respectively. The damping capacity and damping rate of the steel spring floating plate bed at the center of the tunnel are 17.5 dB and 23.3%, respectively. Therefore, the measured results show that the damping effect of the rubber cushion floating plate trackbed is better than that of the steel spring floating plate bed. The numerical simulation results are identical to the measured results.

6. Conclusion

(1) Under the influence of train marshaling, the displacement time history of trackbed presents the distribution law of large in the middle and small at both ends.

(2) The displacement excitation size of the ballast bed is most obviously affected by the damping form of trackbed. The maximum attenuation rate of vertical displacement from steel spring floating plate ballast bed to integral ballast bed is 97.5%. The second is the influence of axle load. When the axle load of the train changes from full load to light load, the maximum attenuation rate of vertical displacement of the trackbed is 35.6%.And finally, the influence of velocity is the smallest influence. When the train speed drops from 80 km/h to 40 km/h, the maximum attenuation rate of vertical displacement of the trackbed is only 7.9%.

(3) Although the integral trackbed had better deformation control ability, its antivibration performance is poor, and the rubber cushion ballast bed has the best antivibration performance, followed by the steel spring floating plate trackbed. The rubber floating cushion trackbed is the ideal ballast bed based on its deformation resistance and vibration reduction effect.

Data Availability

The data used to support the findings of this study are included within the article.

Conflicts of Interest

The authors declare that there are no conflicts of interest regarding the publication of this article.

Acknowledgments

This research was supported by the National Natural Science Foundation of China Youth Fund Project (41702320), the Natural Science Foundation of Shandong Province (ZR202103050706), the Technology Top Talent Support Project of Guizhou Provincial Education Department ([2017]098), and the High-Level Talent Program of Guizhou University of Engineering Science ([G2015]001).

References

[1] P.-P. He and Z.-D. Cui, "Dynamic response of a thawing soil around the tunnel under the vibration load of subway," *Environmental Earth Sciences*, vol. 73, no. 5, pp. 2473–2482, 2015.

[2] J. A. Forrest and H. E. M. Hunt, "A three-dimensional tunnel model for calculation of train-induced ground vibration," *Journal of Sound and Vibration*, vol. 294, no. 4-5, pp. 678–705, 2006.

[3] A. Yaseri, M. H. Bazyar, and S. Javady, "2.5D coupled FEM-SBFEM analysis of ground vibrations induced by train movement," *Soil Dynamics and Earthquake Engineering*, vol. 104, no. 6, pp. 307–318, 2018.

[4] G.-y. Gao, J.-w. Bi, Q.-s. Chen, and R.-m. Chen, "Analysis of ground vibrations induced by high-speed train moving on pile-supported subgrade using three-dimensional FEM," *Journal of Central South University*, vol. 27, no. 8, pp. 2455–2464, 2020.

[5] Z. Zhu, L. Wang, P. A. Costa, Y. Bai, and Z. Yu, "An efficient approach for prediction of subway train-induced ground vibrations considering random track unevenness," *Journal of Sound and Vibration*, vol. 455, no. 9, pp. 359–379, 2019.

[6] H. R. Nejati, M. Ahmadi, H. Hashemolhosseini et al., "Numerical analysis of ground surface vibration induced by underground train movement," *Tunnelling and Underground Space Technology*, vol. 29, no. 5, pp. 1–9, 2012.

[7] L. Wang, Z. Zhu, Q. Li, P. A. Costa, and Z. Yu, "A fast random method for three-dimensional analysis of train-track-soil dynamic interaction," *Soil Dynamics and Earthquake Engineering*, vol. 115, no. 12, pp. 252–262, 2018.

[8] C. Zhu, M. C. He, X. H. Zhang et al., "Nonlinear mechanical model of constant resistance and large deformation bolt and influence parameters analysis of constant resistance behavior," *Rock and Soil Mechanics*, vol. 42, no. 7, pp. 1911–1924, 2021.

[9] Q.-x. Yan, L.-y. Song, H. Chen, W.-y. Chen, S.-q. Ma, and W.-b. Yang, "Dynamic response of segment lining of overlapped shield tunnels under train-induced vibration loads," *Arabian Journal for Science and Engineering*, vol. 43, no. 10, pp. 5439–5455, 2018.

[10] D. P. Connolly, G. Kouroussis, O. Laghrouche, C. L. Ho, and M. C. Forde, "Benchmarking railway vibrations - track, vehicle, ground and building effects," *Construction and Building Materials*, vol. 92, no. 9, pp. 64–81, 2015.

[11] M. Sanayei, J. A. Moore, and C. R. Brett, "Measurement and prediction of train-induced vibrations in a full-scale building," *Engineering Structures*, vol. 77, no. 10, pp. 119–128, 2014.

[12] P. Lopes and J. F. Ruiz, "Vibrations inside buildings due to subway railway traffic. Experimental validation of a comprehensive prediction model," *The Science of the Total Environment*, vol. 568, no. 10, pp. 1333–1343, 2016.

[13] C. Cai, W. Zhai, and K. Wang, "Dynamics simulation of interactions between high-velocity train and Plate track laid on bridge," *China Railway Science*, vol. 25, no. 10, pp. 57–60, 2004.

[14] Z. Dapeng, Q. Liangkai, and L. Yundian, "Analytical study on dynamic response of deep foundation pit support structure under the action of subway train vibration load: a case study of deep foundation pit of the new museum near metro line 2 in chengdu, China," *Shock and Vibration*, vol. 2015, no. 8, pp. 1–10, 2015.

[15] X. L. Ma, Z. N. Ba, Y. H. Gao et al., "Analysis of the influence of subway operation on the vibration of buildings along the coastal soft soil area," *Journal of Rock Mass Engineering*, vol. 41, no. 7, pp. 177–180, 2019.

[16] Y. J. Qiu, X. J. Zhang, and Y. X. Wei, "Influence of train speed on dynamic characteristics of ballastless track subgrade," *Journal of Traffic and Transportation Engineering*, vol. 7, no. 2, pp. 1–5, 2007.

[17] A. M. Kaynia, C. Madshus, and P. Zackrisson, "Ground vibration from high-speed trains: prediction and countermeasure," *Journal of Geotechnical and Geoenvironmental Engineering*, vol. 126, no. 6, pp. 531–537, 2000.

[18] Y. W. Liu, Z. N. Ba, Y. H. Gao et al., "Analysis of the influence of Tianjin Z2 Subway operation on ground vibration," *Journal of Geotechnical Engineering*, vol. 41, no. 7, pp. 193–196, 2019.

[19] L. Han, L. Wang, X. Ding, H. Wen, X. Yuan, and W. Zhang, "Similarity quantification of soil parametric data and sites using confidence ellipses," *Geoscience Frontiers*, vol. 13, no. 1, Article ID 101280, 2022.

[20] Z. X. He, W. M. Qu, and Z. Luo, "Ground vibration caused by subway train," *Journal of Southwest Jiaotong University*, vol. 43, no. 2, pp. 218–221+247, 2008.

[21] D. W. Xie, W. N. Liu, W. F. Liu, and G. Lombaert, "Prediction of influence of subway train vibration on sensitive buildings along the line," *Urban express transit*, vol. 21, no. 1, pp. 44–48, 2008.

[22] P. Liang, Y. T. Gao, and Y. Zhou, "Solution for surrounding rock of strain-softening considering confining pressure-dependent Young's modulus and nonlinear dilatancy," *GEOMECHANICS AND ENGINEERING*, vol. 22, no. 4, pp. 277–290, 2020.

[23] L. Schillemans, "Impact of sound and vibration of the north-south high-speed railway connection through the city of antwerp Belgium," *Journal of Sound and Vibration*, vol. 267, no. 3, pp. 637–649, 2003.

[24] M. Gao, J. Xie, Y. Gao et al., "Mechanical behavior of coal under different mining rates: a case study from laboratory experiments to field testing," *International Journal of Mining Science and Technology*, vol. 31, no. 5, pp. 825–841, 2021.

[25] G. Mingzhong, H. Haichun, L. Tong et al., "Discing behavior and mechanism of cores extracted from Songke-2 well at depths below 4,500 m," *International Journal of Rock Mechanics and Mining Sciences*, vol. 149, no. 1, Article ID 104976, 2022.

[26] G. Li, Y. Hu, S.-m. Tian, M. Weibin, and H.-l. Huang, "Analysis of deformation control mechanism of prestressed anchor on jointed soft rock in large cross-section tunnel," *Bulletin of Engineering Geology and the Environment*, vol. 80, no. 12, pp. 9089–9103, 2021.

[27] L. Han and L. Wang, "Rockhead profile simulation using an improved generation method of conditional random field," *Journal of Rock Mechanics and Geotechnical Engineering*, vol. 13, no. 12, pp. 1674–7755, 2021.

[28] C. Shengai, Z. Bing, H. Zhitang et al., "Application of co-simulation based on multi-body system dynamics and finite element method in coupled vibration research between vehicle and bridge," *Computer Application research*, vol. 26, no. 12, pp. 4581–4584, 2009.

[29] A. N. Huang, Z. M. Yi, and A. Q. Zhang, "Dynamic total energy simulation analysis of rail vehicles based on SIMPACK," *Machinery & Electronics*, vol. 51, no. 3, pp. 77–80, 2013.

[30] W. Kortüm, "Review of multibody computer, codes for vehicle system dynamics," *Vehicle System Dynamics*, vol. 22, no. sup1, pp. 3–31, 1993.

[31] R. L. Huston, C. E. Passerello, and M. W. Harlow, "Dynamics of multirigid-body systems," *Journal of Applied Mechanics*, vol. 45, no. 4, pp. 889–894, 1978.

[32] C. N. Li, *Dynamics Study of Track Bedless Turnout on High-Velocity Railway Bridge Based on Joint Simulation of Rigid and Flexible Coupling*, Beijing Jiaotong University, Beijing, 2011.

[33] J. B. Yao, *Dynamic Characteristics Analysis of Subway Steel-spring Floating Plate Track Bed*, Lanzhou Jiaotong University, Lanzhou, China, 2017.

[34] F. Xu, Q. Yang, W. Liu, W. Leng, R. Nie, and H. Mei, "Dynamic stress of subgrade bed layers subjected to train vehicles with large axle loads," *Shock and Vibration*, vol. 2018, no. 5, pp. 1–12, Article ID 2916096, 2018.

[35] J. Liu, Z. Guo, X. Ling, X. Yu, and N. Zhu, "Studies on bearing characteristic of open-ended and close-ended pipe piles under high-speed railway loadings," *International Journal of Structural Stability and Dynamics*, vol. 21, no. 14, Article ID 2140001, 2021.